

Effects of humid air on aerodynamic journal bearings

Eliott Guenat¹, Jürg Schiffmann

*Ecole Polytechnique Fédérale de Lausanne, Laboratory for applied mechanical design,
Maladière 71b, CP 526, CH-2002 Neuchâtel 2*

Abstract

The development of aerodynamic bearings applications where ambient conditions cannot be controlled (e.g., for automotive fuel cell compressor) raises the question of the effects of condensation in the humid air on performance. A modified Reynolds equation is obtained in relation to humid air thermodynamic equations, accounting for the variation of compressibility and viscosity in the gas mixture. The load capacity and stability of plain and herringbone-grooved journal bearings is computed on a wide range of operating and ambient conditions. In general, performance metrics show an independence on humid-air effects at moderated temperature, although the stability of the grooved journal bearing exhibits strong variations in particular conditions. In consequence, a safety margin of 25% is suggested for the critical mass.

Keywords: Aerodynamic Lubrication, Gas Bearings, Humid air, Simulation

¹Corresponding author. Email adress: eliott.guenat@epfl.ch

Roman symbols

a	Groove length
b	Ridge length
C	Damping coefficient
c_s	NGT coefficient
c	Viscosity coefficient
\tilde{c}	Molar concentration
D	Bearing diameter
e	Eccentricity
f	NGT coefficient
g	NGT coefficient
H	Groove depth ratio h_g/h_0 at $\epsilon = 0$
h	Clearance
h_0	Nominal clearance
h_g	Groove clearance
h_r	Ridge clearance
L	Bearing length
M_c	Critical mass
M_r	Critical mass ratio
\tilde{m}	Molar mass
P	Pressure
R	Radius
r	Specific gas constant
T	Temperature
t	Time
U	Bearing tangential velocity
W	Load capacity
W_r	Load capacity ratio
w	Humidity ratio
X	Coordinate in the direction of the displacement
x	Coordinate in the inertial frame
y	Coordinate in the inertial frame
z	Axial coordinate
Greek symbols	
α	Groove aspect ratio
β	Bulk modulus
$\hat{\beta}$	Groove angle

ϵ	Eccentricity ratio
θ	Circumferential coordinate
Λ	Compressibility number
μ	Dynamic viscosity
ρ	Density
σ	Squeeze number
Φ	Viscosity coefficient
ϕ	Relative humidity
Ω	Bearing angular velocity
ω	Excitation angular velocity
	Superscripts
—	Normalized
*	Saturated
	Subscripts
<i>a</i>	Ambient condition
<i>air</i>	Air
<i>c</i>	Critical
<i>cond</i>	Condensable
<i>g</i>	Groove
<i>non – cond</i>	Non-condensable
<i>r</i>	Ridge, ratio
<i>T</i>	Isothermal
<i>vap</i>	Water vapor (gas phase)
<i>w</i>	Water liquid phase
<i>x</i>	<i>x</i> -axis
<i>y</i>	<i>y</i> -axis
<i>z</i>	<i>z</i> -axis
0	Static, unperturbed
1	Perturbed
	Acronyms
<i>HA</i>	Humid air
<i>HGJB</i>	Herringbone grooved journal bearing
<i>PJB</i>	Plain journal bearing
<i>NGT</i>	Narrow groove theory

1. Introduction

The use of aerodynamic bearings expands progressively to domains where the ambient conditions cannot be satisfactorily conditioned, either due to economical or to technical reasons. In particular, gas bearing-supported pressurizers of Proton-Exchange Membrane (PEM) fuel cells [1] for automotive applications are subject to a large range of ambient temperatures and relative humidities. Thus, the knowledge of the effect of ambient humidity on the performance of an aerodynamic bearing is necessary to ensure the viability of a given design.

1.1. Nature of the issue

Water vapor contained in humid air (HA) is subject to condensation if the saturation pressure is reached within the fluid film of gas-lubricated bearings. The resulting effects might influence the bearing behavior. Several works [2, 3] theoretically and experimentally investigated the influence of HA on the static pressure field of hard disk drive heads, showing that vapor condensation can occur, which reduces the pressure in the bearing, leading to a reduction of the head's flying height. For the same application, Hua et al. [4] performed transient simulations investigating the settling time of the flying head and showed that HA effects affect the final state of the bearing. In the previously mentioned works, the simulation method to model HA effects consists in applying a correction on the pressure field obtained from the ideal-gas form of the Reynolds equation. Kirpekar et al. [5] introduced a modification of the Reynolds equation to obtain a more rigorous approach. However, the existing literature on the HA-lubricated bearings is limited to slider geometries with ultra-thin film lubrication, with no application to journal bearings.

1.2. Goals and objectives

The present work investigates the HA effects on the performance of plain journal bearings (PJB) and of herringbone-grooved journal bearings (HGJB). The objectives are to: (1) develop an expression of the Reynolds equation for HA-lubricated journal bearings, (2) evaluate the deviation of HA-lubricated journal bearing from ideal-gas lubrication in terms of load capacity and whirl stability in a large range of ambient temperatures, relative humidities and operating conditions and (3) devise design guidelines for robust design considering HA effects.

36 *1.3. Scope of the Paper*

37 The Reynolds equation for compressible fluids is adapted to express the
38 local density, exhibiting the bulk modulus whose expression depends on
39 whether the saturation conditions are locally met or not. The expression
40 of the bulk modulus is derived from the classical humid air theory and ac-
41 counts for the drying effect of condensing vapor. The perturbation method
42 is applied on the Reynolds equation and a finite difference scheme is used
43 to solve the equations. Static and dynamic bearing properties are obtained
44 by integrating the pressure fields. The concept of critical mass is used as a
45 stability metric regarding the whirl instability. The deviation of HA lubrica-
46 tion from the ideal-gas case is investigated for both PJB and HGJB in terms
47 of load capacity and critical mass. The selected HGJB geometry maximizes
48 the stability at moderated compressibility number ($\Lambda = 1$). The consid-
49 ered operating conditions vary in temperature from 275 to 370 K, in relative
50 humidity from 0 to 1 with different eccentricity ratios and compressibility
51 numbers up to 30. Based on the generated results, a set of design guidelines
52 is suggested for the design of HA-lubricated journal bearings based on the
53 ideal-gas Reynolds equation.

54 **2. Theory**

55 HA lubrication implies a condensable gas mixture of water (condensable)
56 and air, considered as incondensable. The main working hypotheses in the
57 following development are: (1) the gas film is isothermal, (2) the thermody-
58 namic equilibrium is instantaneous as suggested by Ma et Liu [6], (3) only the
59 gas phase is considered. The hypothesis (1) is justified by the large contact
60 area of the gas film with the rotor and bushings. These areas are heteroge-
61 neous nucleation sites justifying (2) and the very small volume of condensed
62 water regarding the gas phase justifies (3). The Reynolds equation adds the
63 hypothesis of thin film, laminar flow, Newtonian fluid and negligible inertial
64 effects. It is recalled as follows:

$$\partial_X \left(\frac{\rho h^3}{12\mu} \partial_X P \right) + \partial_z \left(\frac{\rho h^3}{12\mu} \partial_z P \right) = \frac{U}{2} \partial_X(\rho h) + \partial_t(\rho h) \quad (1)$$

65 Since the practical problem targeted in the present work involves an at-
66 mospheric pressure, both gases (air and water vapor) are considered as ideal.
67 However, for an isothermal gas, the saturation partial pressure of water can
68 be reached within the film as mixture pressure increases. At this point (dew

69 point), water vapor starts condensing and limits its contribution to the mix-
 70 ture pressure build-up on which the bearing relies to serve its purpose. At
 71 this point, the behavior of the mixture deviates from an ideal gas, namely:

$$P = \rho r_a T \quad (2)$$

72 where r_a is the specific gas constant of the ambient HA. In order to account
 73 for this deviation, Equation 2 is not used to substitute the density with the
 74 pressure in Reynolds equation. Instead, the following changes of variable are
 75 applied:

$$\frac{\partial P}{\partial X} = \left(\frac{\partial P}{\partial \rho} \right)_T \cdot \frac{\partial \rho}{\partial X}, \quad \frac{\partial P}{\partial z} = \left(\frac{\partial P}{\partial \rho} \right)_T \cdot \frac{\partial \rho}{\partial z} \quad (3)$$

76 Where $(\partial_\rho P)_T$ is associated to the bulk modulus β of the lubricant gas:

$$\rho \left(\frac{\partial P}{\partial \rho} \right)_T = \beta \quad (4)$$

77 The following normalization is performed on Equation 1 to express it in
 78 cylindrical coordinates (Equation 6):

$$\begin{aligned} \bar{\rho} &= \rho/\rho_a & \bar{\mu} &= \mu/\mu_a & \bar{\beta} &= \beta/P_a & \theta &= X/R \\ \bar{z} &= z/R & \bar{h} &= h/h_0 & \bar{t} &= t\omega \end{aligned} \quad (5)$$

$$\partial_\theta \left(\frac{\bar{\beta} \bar{h}^3}{\bar{\mu}} \partial_\theta \bar{\rho} \right) + \partial_{\bar{z}} \left(\frac{\bar{\beta} \bar{h}^3}{\bar{\mu}} \partial_{\bar{z}} \bar{\rho} \right) = \Lambda \partial_\theta (\bar{\rho} \bar{h}) + \sigma \partial_{\bar{t}} (\bar{\rho} \bar{h}) \quad (6)$$

79 Where Λ and σ are the compressibility and squeeze number respectively,
 80 defined as follows for journal bearings (Figure A.1):

$$\Lambda = \frac{6\mu_a \Omega R^2}{P_a h_0^2} \quad (7)$$

$$\sigma = 2\Lambda \frac{\omega}{\Omega} \quad (8)$$

In order to obtain the dynamic coefficients and to compute the critical mass, the clearance is perturbed by an infinitesimal harmonic motion ϵ_{1x} and ϵ_{1y} ($\epsilon_{x/y} = e_{x/y}/h_0$) in the x and y directions respectively [7]:

$$\bar{h} = \bar{h}_0 - \epsilon_{1x} \cos \theta e^{i\bar{t}} - \epsilon_{1y} \sin \theta e^{i\bar{t}} \quad (9)$$

$$= 1 - \epsilon_{0x} \cos \theta - \epsilon_{0y} \sin \theta - \epsilon_{1x} \cos \theta e^{i\bar{t}} - \epsilon_{1y} \sin \theta e^{i\bar{t}} \quad (10)$$

81 where ϵ_{0x} and ϵ_{0y} are the static equilibrium eccentricity ratios. The other
 82 perturbed terms involved in Equation 7 are:

$$\bar{\rho} = \bar{\rho}_0 + \epsilon_{1x}\bar{\rho}_{1x}e^{i\bar{t}} + \epsilon_{1y}\bar{\rho}_{1y}e^{i\bar{t}} \quad (11)$$

$$\bar{\beta} = \bar{\beta}_0 + \epsilon_{1x} \left(\frac{\partial \bar{\beta}}{\partial \bar{\rho}} \right)_0 \bar{\rho}_{1x}e^{i\bar{t}} + \epsilon_{1y} \left(\frac{\partial \bar{\beta}}{\partial \bar{\rho}} \right)_0 \bar{\rho}_{1y}e^{i\bar{t}} \quad (12)$$

$$\frac{1}{\bar{\mu}} = \frac{1}{\bar{\mu}_0} + \epsilon_{1x} \left(\frac{-1}{\bar{\mu}^2} \frac{\partial \bar{\mu}}{\partial \bar{\rho}} \right)_0 \bar{\rho}_{1x}e^{i\bar{t}} + \epsilon_{1y} \left(\frac{-1}{\bar{\mu}^2} \frac{\partial \bar{\mu}}{\partial \bar{\rho}} \right)_0 \bar{\rho}_{1y}e^{i\bar{t}} \quad (13)$$

83 Only terms of order 0 and 1 with respect to ϵ_{1x} and ϵ_{1y} are retained
 84 and grouped in Equations 14 and 15 respectively. The same procedure is
 85 reiterated in the y direction without being repeated here.

$$\partial_\theta \left[\frac{\bar{\beta}_0 \bar{h}_0^3}{\bar{\mu}_0} \partial_\theta \bar{\rho}_0 \right] + \partial_z \left[\frac{\bar{\beta}_0 \bar{h}_0^3}{\bar{\mu}_0} \partial_z \bar{\rho}_0 \right] - \Lambda \partial_\theta (\bar{\rho}_0 \bar{h}_0) = 0 \quad (14)$$

$$\begin{aligned} & \partial_\theta \left[\left(\frac{\partial \bar{\beta}}{\partial \bar{\rho}} \right)_0 \bar{\rho}_{1x} \frac{\bar{h}_0^3}{\bar{\mu}_0} \partial_\theta \bar{\rho}_0 + \bar{\beta}_0 \left(\frac{-1}{\bar{\mu}^2} \frac{\partial \bar{\mu}}{\partial \bar{\rho}} \right)_0 \bar{\rho}_{1x} \bar{h}_0^3 \partial_\theta \bar{\rho}_0 + \right. \\ & \quad \left. \frac{\bar{\beta} \bar{h}_0^2}{\bar{\mu}_0} \cos \theta \partial_\theta \bar{\rho}_0 + \frac{\bar{\beta}_0 \bar{h}_0^3}{\bar{\mu}_0} \partial_\theta \bar{\rho}_{1x} \right] \\ & + \partial_z \left[\left(\frac{\partial \bar{\beta}}{\partial \bar{\rho}} \right)_0 \bar{\rho}_{1x} \frac{\bar{h}_0^3}{\bar{\mu}_0} \partial_\theta \bar{\rho}_0 + \bar{\beta}_0 \left(\frac{-1}{\bar{\mu}^2} \frac{\partial \bar{\mu}}{\partial \bar{\rho}} \right)_0 \bar{\rho}_{1x} \bar{h}_0^3 \partial_\theta \bar{\rho}_0 + \right. \\ & \quad \left. \frac{\bar{\beta} \bar{h}_0^2}{\bar{\mu}_0} \cos \theta \partial_\theta \bar{\rho}_0 + \frac{\bar{\beta}_0 \bar{h}_0^3}{\bar{\mu}_0} \partial_\theta \bar{\rho}_{1x} \right] \\ & - \Lambda \partial_\theta (\bar{\rho}_0 \cos \theta + \bar{\rho}_{1x} \bar{h}_0) - i\sigma (\bar{\rho}_0 \cos \theta + \bar{\rho}_{1x} \bar{h}_0) = 0 \end{aligned} \quad (15)$$

86 A central finite difference scheme is employed to discretize the equations with
 87 the boundary conditions of periodicity for $\theta = 0$ and $\theta = 2\pi$ and ambient
 88 density at $\bar{z} = \pm L/D$. The procedure consists in solving successively both
 89 unperturbed and perturbed equations to obtain the corresponding pressure
 90 fields, integrating them over the bearing domain to get the load capacity and
 91 complex impedances leading to the computation of the critical mass [8].

92 The same method can be applied to the HGJB using the Narrow Groove
 93 Theory (NGT) to obtain a modified Reynolds equation [9]. This procedure
 94 predicts the overall pressure generated by an infinite number of groove-ridge

95 pairs over the bearing domain, smoothing the local pressure variation over a
 96 ridge-groove pair. Only the resulting differential equation is displayed here:

$$\begin{aligned}
 & \partial_\theta [\bar{\beta} (f_1 \partial_\theta \bar{\rho} + f_2 \partial_z \bar{\rho})] + \partial_z [\bar{\beta} (f_2 \partial_\theta \bar{\rho} + f_3 \partial_z \bar{\rho})] \\
 & + c_s \left(\sin \hat{\beta} \partial_\theta (f_4 \bar{\rho}) - \cos \hat{\beta} \partial_z (f_4 \bar{\rho}) \right) \\
 & - \Lambda \partial_\theta (f_5 \bar{\rho}) - \sigma \partial_{\hat{t}} (f_5 \bar{\rho}) = 0
 \end{aligned} \tag{16}$$

97 where the geometry is presented in Figure A.2 and functions f_i are sum-
 98 marized in the Appendix. A first-order perturbation is applied to this equa-
 99 tion following Equations 9 to 13 and zeroth- and first-order equations are
 100 segregated to be solved successively.

101 The problem of HA lubrication consists in the expression of $(\partial_{\bar{\rho}} \bar{P})_T$. As
 102 long as the saturation partial pressure of water vapor is not locally reached,
 103 the mixture is assumed to be an ideal gas. Thus, the term $(\partial_{\bar{\rho}} \bar{P})_T$, encapsu-
 104 lated in the bulk modulus, is equal to unity:

$$(\partial_{\bar{\rho}} \bar{P})_T = \frac{\rho_a}{P_a} (\partial_\rho P)_T = \frac{\rho_a r_a T}{P_a} = 1 \tag{17}$$

105 Only when the saturation pressure is met, condensing water will stop
 106 building up pressure, leading to $(\partial_{\bar{\rho}} \bar{P})_T < 1$, thus, departing from the ideal-
 107 gas behavior.

108 The ideal-gas equation for the gas mixture is:

$$P = \rho r T \tag{18}$$

109 The value of $(\partial_\rho P)_T$ is simply:

$$(\partial_\rho P)_T = r T + \rho T \partial_\rho r \tag{19}$$

110 where r is the mixture specific gas constant

$$r = \frac{r_{air} + w r_{vap}}{1 + w} \tag{20}$$

111 and w is the humidity ratio defined as the ratio of mass water vapor per unit
 112 mass of dry air:

$$w = \frac{M_{vap}}{M_{air}} \tag{21}$$

113 The value of w of the gas phase is defined locally depending on whether the
 114 saturation conditions are met or not:

$$w = \min(w_a, w^*(T_a, P)) \quad (22)$$

115 w^* is the saturation humidity ratio, which is a function of the ambient tem-
 116 perature and local pressure as follows:

$$w^* = \frac{\tilde{m}_{vap} P_{vap}^*(T_a)}{\tilde{m}_{air} P - P_{vap}^*(T_a)} \quad (23)$$

117 where P_{vap}^* is the saturation pressure of water that depends on the tempera-
 118 ture only, computed using a fluid database [10]. Since Equation 6 deals with
 119 density rather than pressure, it is convenient to have an expression of w^* as
 120 a function of density. For that purpose Equation 18 is inserted in Equation
 121 23 and w^* is isolated:

$$w^* = \frac{-c_2 + \sqrt{c_2^2 - 4c_1c_3}}{2c_1} \quad (24)$$

122 with

$$c_1 = (\rho r_{vap} T - P_{vap}^*) \quad (25)$$

$$c_2 = r_{air} \rho T - P_{vap}^* (1 + \tilde{m}_{vap}/\tilde{m}_{air}) \quad (26)$$

$$c_3 = P_{vap}^* \tilde{m}_{vap}/\tilde{m}_{air} \quad (27)$$

123 If saturation is reached and the water content in the gas phase decreases,
 124 the mixture viscosity evolves accordingly. It is expressed from [11] as follows:

$$\mu = \frac{(1 - \tilde{c}_{vap}) - \mu_{air}}{1 - \tilde{c}_{vap} + \tilde{c}_{vap} \Phi_{av}} + \frac{\tilde{c}_{vap} \mu_{vap}}{\tilde{c}_{vap} + (1 - \tilde{c}_{vap}) \Phi_{va}} \quad (28)$$

125 where

$$\Phi_{av} = \frac{\sqrt{2}}{4} \left(1 + \frac{\tilde{m}_{air}}{\tilde{m}_{vap}}\right)^{-0.5} \left(1 + \left(\frac{\mu_{air}}{\mu_{vap}}\right)^{0.5} \left(\frac{\tilde{m}_{vap}}{\tilde{m}_{air}}\right)^{0.25}\right)^2 \quad (29)$$

$$\Phi_{va} = \frac{\sqrt{2}}{4} \left(1 + \frac{\tilde{m}_{vap}}{\tilde{m}_{air}}\right)^{-0.5} \left(1 + \left(\frac{\mu_{vap}}{\mu_{air}}\right)^{0.5} \left(\frac{\tilde{m}_{air}}{\tilde{m}_{vap}}\right)^{0.25}\right)^2 \quad (30)$$

126 \tilde{c}_{vap} is the molar concentration of water vapor in the gas phase, related to
 127 the humidity ratio as follows:

$$\tilde{c}_{vap} = \frac{1}{1 + \frac{\tilde{m}_{vap}}{w\tilde{m}_{air}}} \quad (31)$$

128 The deviation from the ideal-gas law and the change of viscosity provide the
 129 necessary tools for the modeling of HA-lubricated journal bearings.

130 3. Numerical computations and results

131 Journal bearings lubricated with condensable humid air are compared to
 132 equivalent non-condensable (ideal gas) cases using two performance metrics,
 133 namely the load capacity ratio W_r and the critical mass ratio M_r , defined as
 134 follows:

$$W_r = \frac{W_{cond}}{W_{non-cond}} \quad (32)$$

$$M_r = \frac{M_{c,cond}}{M_{c,non-cond}} \quad (33)$$

$$(34)$$

135 Both the investigated geometries have a L/D ratio of 1. Moreover, the
 136 HGJB geometry is based on the design obtained in [12] maximizing the min-
 137 imal critical mass for the range $\Lambda \in [0, 1]$ (Equation 39) when the grooved
 138 member rotates:

$$\alpha = 0.6 \quad (35)$$

$$\hat{\beta} = 145.8^\circ \quad (36)$$

$$H = 2.25 \quad (37)$$

139 Unless specified differently, the simulations presented below are performed
 140 at an ambient temperature of 308 K, which is assumed to represent a pes-
 141 simistic temperature for humid environments. A first simulation of the PJB
 142 running at $\Lambda = 30$, and $\epsilon_x = 0.5$ allows to understand the consequences of
 143 humid air lubrication. Figure A.3 presents the pressure relative to the ambi-
 144 ent at the mid-span of the considered bearing and the relative deviation of

145 the pressure compared to the non-condensable case with an ambient relative
 146 humidity of 0.8. The relative humidity ϕ is defined as follows:

$$\phi = \frac{P_{vap}}{P_{vap}^*} \quad (38)$$

147 The pressure is not only affected in the zone where it exceeds the dew
 148 point, exhibiting a reduction exceeding 0.8% , but also outside this zone,
 149 although the deviation is even more modest. The pressure field is globally
 150 affected because of the elliptical characteristic of the Reynolds equation, the
 151 value at one given point affecting the entire fluid film domain. This kind of
 152 observation is impossible with HA effects considered *a posteriori*, on top of
 153 the computed pressure field with non-condensable gas lubrication, as usually
 154 seen in the literature [2, 3, 4].

155 Figure A.4 presents the isolines of the load capacity ratio W_r for the
 156 PJB at $\epsilon_x = 0.5$ as a function of the ambient relative humidity ϕ_a and
 157 the compressibility number Λ . Load capacity drops when the saturation is
 158 reached inside the bearing, and the condensation onset is reached at lower
 159 values of ϕ_a as Λ increases, until it converges toward a limit value. This
 160 is due to the well-known limiting solution for PJB with $\Lambda \rightarrow \infty$, at which
 161 a limit pressure field is reached. With a maximum relative deviation of
 162 approximately 1.5% at this ambient temperature, the loss of load capacity
 163 remains low at all values of compressibility number, even at high ambient
 164 relative humidity. Deviation of this order of magnitude can be considered as
 165 negligible from a practical point of view.

166 Figure A.5 depicts the evolution of M_r with ϕ_a and Λ . Once saturation
 167 is reached within the gas film, the condensation effects have a small yet neg-
 168 ative influence on M_r . Such a modest evolution of the critical mass remains
 169 without consequences on the practical design and performance of a PJB.

170 Figures A.6 and A.7 present the same approach with the HGJB for W_r
 171 and M_r respectively, at $\epsilon_x = 0.05$. The load capacity is negatively affected by
 172 the condensation, with a maximum deviation of less than 1%. Regarding the
 173 stability in the saturated domain, M_r is above unity on the left side of the line
 174 $\Lambda \approx 9$ and below unity on its right side. The largest low- and high-deviation
 175 values are reached at the line itself, with a very abrupt change of trend.
 176 The underlying phenomenon is the point of very high stability observed for
 177 HGJB for particular values of Λ . Under the condition of saturated humid
 178 air lubrication, the position of this stability peak is shifted to slightly lower
 179 values of Λ (Figure A.8), explaining the abrupt variation of M_r in this zone,

180 whose amplitude rises with the ambient relative humidity (the 25%-deviation
 181 lines diverge along the ϕ_a axis). However, M_r gets close to 1 as soon as the
 182 operating conditions deviate from this particular zone.

183 From a design perspective, the minimum value of the critical mass be-
 184 tween the targeted value of compressibility number Λ^* and 0 bears a par-
 185 ticular importance, since it indicates the stability threshold of a bearing
 186 accelerating from rest to nominal speed. A new metric is defined to compare
 187 the minimal value of the critical mass in this range:

$$M_{r,min} = \frac{\min_{\Lambda \in [0, \Lambda^*]} M_{c,cond}}{\min_{\Lambda \in [0, \Lambda^*]} M_{c,non-cond}} \quad (39)$$

188 Figure A.9 depicts the evolution of M_r and $M_{r,min}$ with Λ^* for the saturated
 189 ambient condition ($\phi_a = 1$). The improvement of critical mass observed
 190 for the condensable lubrication on the left-hand side of the turn-over point
 191 at $\Lambda^* \approx 9$ is translated into a moderately improved value of the minimum
 192 critical mass ($\approx 3\%$). Past this point, $M_{r,min}$ coincides with the line of M_r ,
 193 resulting in a depreciation of the minimum critical mass reaching 25%, which
 194 is not negligible from a design perspective.

195 The effects of the eccentricity ratio on the considered bearings are pre-
 196 sented in Figure A.10, at $\Lambda = 10$ and $\phi_a = 0.9$. The evolution of W_r shows
 197 no clear trend for the HGJB and diminishes for the PJB as soon as the
 198 saturation point is reached, yet in an insignificant order of magnitude. The
 199 value of M_r for the HGJB increases slightly because of the further shift in the
 200 critical mass curve. The M_r of the PJB shows a local minimum at $\epsilon_x \approx 0.17$,
 201 however at levels without practical implications. Both metrics for HGJB are
 202 affected by humid-air effects already at a concentric position because of the
 203 inherent pressure build-up due to the grooved pattern, while saturation is
 204 reached only above $\epsilon_x \approx 0.1$ for the PJB.

205 Figure A.11 presents the evolution of the minimum value of $M_{r,min}$ for
 206 $\Lambda^* = 50$ with the eccentricity ratio, in saturated ambient conditions. This
 207 metric shows a minimum at concentric position and relaxes as the eccentricity
 208 ratio increases.

209 The effects of the ambient temperature are presented in Figure A.12 for
 210 both PB and HGJB at $\phi_a = 0.9$. The concentration of water in the gas
 211 mixture increases with temperature at equal value of relative humidity, thus
 212 enhancing the effects of humid-air lubrication at high ambient temperature.

213 All metrics are affected in significant proportions at temperatures approach-
 214 ing 100 °C. The strong enhancement of M_r for the HGJB is due to the fact
 215 that the stability peak is shifted to lower values of Λ as the temperature
 216 increases with constant ϕ_a . For both bearings, the load capacity is reduced
 217 by 2% at a temperature of 330 K. On the same Figure the minimum value of
 218 $M_{r,min}$ for $\Lambda^* = 50$ and in saturated ambient conditions is shown in order to
 219 represent the worst case scenario. The temperature has a significant influ-
 220 ence, since this indicator approaches 0 near 100 °C. The humid air effects are
 221 still significant on this indicator at lower temperatures, since the 10%-losses
 222 threshold is located at 290 K.

223 The influence of liquid water droplets formed in the bearing clearance
 224 due to condensation can be questioned, since the formation of a liquid phase
 225 in the lubrication film can threaten the viability of the bearing. However,
 226 because of its significant difference of density at near-normal conditions (three
 227 orders of magnitude), the liquid phase, which was neglected in the previous
 228 computations, might occupy an insignificant volume in the mixture. In order
 229 to analyze this, the void fraction, defined as the volume of gas phase over
 230 the total two-phase volume, is used:

$$\delta = \frac{v_{gas}}{v_{liquid} + v_{gas}} \quad (40)$$

231 Figure A.13 shows the "1-void fraction" of the mixture for different ambient
 232 temperature and $\phi_a = 1$ in the situation where all the water from the sat-
 233 urated solution condenses, which is an overestimation of reality. Under this
 234 assumption, the void fraction gets the following expression:

$$\delta = \frac{1}{1 + w_a \rho_{air} / \rho_w} \quad (41)$$

235 The minimum value barely reaches 99% for T just below 100 °C, which is
 236 suggested to be sufficiently small to discard any risk linked to the formation
 237 of a local liquid film in the bearing clearance.

238 4. Conclusions

239 A modified form of the Reynolds equation suited for humid-air lubrica-
 240 tion was developed and applied to grooved and plain journal bearings on
 241 a wide range of operating conditions (compressibility number, eccentricity

242 ratio, ambient temperature and relative humidity). Cases accounting for va-
243 por condensation in the lubrication film were compared to non-condensable
244 cases (ideal gas) in terms of load capacity and stability (critical mass). The
245 investigations lead to the following observations:

- 246 • Humid air (HA) lubrication affects the pressure distribution in a lubri-
247 cation gas film even at locations where the pressure does not exceed
248 the dew pressure
- 249 • Consequences of HA lubrication are in general more significant at high
250 compressibility numbers Λ , ambient humidity ratios and eccentricity
251 ratios. High levels of ambient temperature increase the sensitivity of
252 load capacity and stability to humid-air effects, as the mass concentra-
253 tion of water in air increases
- 254 • Herringbone-grooved journal bearings (HGJB) are more sensitive to
255 HA effects than plain journal bearings (PJB), notably because of their
256 inherent pressure build-up even at concentric position, whereas PJBs
257 require a higher eccentricity to develop HA effects.
- 258 • Vapor condensation negatively affects the load capacity of journal bear-
259 ings, however without practical significance at temperature levels met
260 in atmospheric conditions ($T_a < 310$ K). The critical mass of PJBs is
261 affected in negligible proportions, while HGJBs can experience a signifi-
262 cantly reduced critical mass at particular compressibility numbers, with
263 a reported reduction up to 25% in realistic atmospheric temperatures.
264 In consequence, an equivalent margin is suggested on the critical mass
265 to ensure a safe operation of HGJBs designed from the non-condensable
266 Reynolds equation.
- 267 • In realistic situations, the presence of liquid droplets in the bearing
268 clearance is unlikely to be a threat to the integrity of the system due
269 to the very small void fraction calculated in worst-case scenarii.

270 **Acknowledgment**

271 The first author would like to thank Ms.Oihénart for the provided sup-
272 port. The authors acknowledge the funding by the Swiss National Science
273 Foundation, grant PYAPP2_154278/1.

274 **Reference**

- 275 [1] B. Blunier, A. Miraoui, Air management in PEM fuel cells: State-of-
276 the-art and prospectives, in: 2007 International Aegean Conference on
277 Electrical Machines and Power Electronics, pp. 245–254.
- 278 [2] B. Strom, Shuyu Zhang, Sung Chang Lee, A. Khurshudov, G. Tyndall,
279 Effects of Humid Air on Air-Bearing Flying Height, IEEE Transactions
280 on Magnetics 43 (2007) 3301–3304.
- 281 [3] S. Zhang, B. Strom, S.-C. Lee, G. Tyndall, Simulating the Air Bear-
282 ing Pressure and Flying Height in a Humid Environment, Journal of
283 Tribology 130 (2008) 011008.
- 284 [4] W. Hua, W. Zhou, B. Liu, S. Yu, C. H. Wong, Effect of environment
285 humidity and temperature on stationary and transient flying responses
286 of air bearing slider, Tribology International 42 (2009) 1125–1131.
- 287 [5] S. Kirpekar, O. Ruiz, Computing the performance of an air bearing in
288 humid conditions, Applied Physics Letters 94 (2009) 234103.
- 289 [6] Y. Ma, B. Liu, Contribution of water vapor to slider air-bearing pressure
290 in hard disk drives, Applied Physics Letters 90 (2007) 223502.
- 291 [7] J. W. Lund, Calculation of Stiffness and Damping Properties of Gas
292 Bearings, Journal of Lubrication Technology 90 (1968) 793–803.
- 293 [8] E. Guenat, J. Schiffmann, Real-gas effects on aerodynamic bearings,
294 Tribology International 120 (2018) 358–368.
- 295 [9] J. H. Vohr, C. Y. Chow, Characteristics of Herringbone-Grooved, Gas-
296 Lubricated Journal Bearings, Journal of Basic Engineering 87 (1965)
297 568–576.
- 298 [10] I. H. Bell, J. Wronski, S. Quoilin, V. Lemort, Pure and Pseudo-pure
299 Fluid Thermophysical Property Evaluation and the Open-Source Ther-
300 mophysical Property Library CoolProp, Industrial & Engineering Chem-
301 istry Research 53 (2014) 2498–2508.
- 302 [11] P. Tsilingiris, Thermophysical and transport properties of humid air
303 at temperature range between 0 and 100C, Energy Conversion and
304 Management 49 (2008) 1098–1110.

305 [12] D. P. H. Fleming, Optimization of self-acting herringbone journal bear-
 306 ings for maximum stability, in: International Gas Bearing Symposium,
 307 Mar. 26-29, 1974, Southampton.

308 Appendix A. Turbulent NGT

309 The terms composing equation 16 are developed here.

$$\bar{h}_r = \frac{h_r}{h_0} = \frac{h_r}{h_r(\epsilon = 0)} \quad (\text{A.1})$$

$$\bar{h}_g = \frac{h_g}{h_0} \quad (\text{A.2})$$

$$H = \frac{h_g(\epsilon = 0)}{h_0} \quad (\text{A.3})$$

$$g_1 = \bar{h}_g^3 \bar{h}_r^3 \quad (\text{A.4})$$

$$g_2 = (\bar{h}_g^3 - \bar{h}_r^3)^2 \alpha (1 - \alpha) \quad (\text{A.5})$$

$$g_3 = (1 - \alpha) \bar{h}_g^3 + \alpha \bar{h}_r^3 \quad (\text{A.6})$$

$$c_s = - \frac{6\mu\Omega R^2}{p_a h_0^2} \alpha (1 - \alpha) (H - 1) \sin \hat{\beta} \quad (\text{A.7})$$

$$f_1 = \frac{g_1 + g_2 \sin^2 \hat{\beta}}{g_3} \quad (\text{A.8})$$

$$f_2 = \frac{g_2 \sin \hat{\beta} \cos \hat{\beta}}{g_3} \quad (\text{A.9})$$

$$f_3 = \frac{g_1 + g_2 \cos^2 \hat{\beta}}{g_3} \quad (\text{A.10})$$

$$f_4 = \frac{\bar{h}_g^3 - \bar{h}_r^3}{g_3} \quad (\text{A.11})$$

$$f_5 = \alpha \bar{h}_g + (1 - \alpha) \bar{h}_r \quad (\text{A.12})$$

310 **List of Figures**

311 A.1 Nomenclature of a journal bearing 18
312 A.2 Geometry and nomenclature of a HGJB 19
313 A.3 Relative pressure and deviation along the circumference of a
314 PJB at $\bar{z} = 0$, $\epsilon_x = 0.5$, $\phi_a = 0.8$ and $\Lambda = 30$) 20
315 A.4 Isolines of W_r for PJB at $\epsilon_x = 0.5$ ($T_a = 308$ K) 21
316 A.5 Isolines of M_r for PJB at $\epsilon_x = 0.5$ ($T_a = 308$ K) 22
317 A.6 Isolines of W_r for HGJB at $\epsilon_x = 0.05$ ($T_a = 308$ K) 23
318 A.7 Isolines of M_r for HGJB at $\epsilon_x = 0.05$ ($T_a = 308$ K) 24
319 A.8 Critical mass for HGJB at $\epsilon_x = 0.05$ ($T_a = 308$ K, $\phi_a = 1$) as
320 a function of Λ with and without vapor condensation 25
321 A.9 M_r and $M_{r,min}$ for HGJB at $\epsilon_x = 0.05$ ($T_a = 308$ K, $\phi_a = 1$)
322 as a function of Λ 26
323 A.10 Evolution of W_r and M_r for HGJB and PJB with the eccen-
324 tricity ratio ($T_a = 308$ K, $\Lambda = 5$, $\phi_a = 0.9$) 27
325 A.11 Evolution of the minimum value of $M_{r,min}$ for $\Lambda^* = 50$ with
326 the eccentricity ratio for HGJB ($T_a = 308$ K, $\phi_a = 1$) 28
327 A.12 Evolution of W_r and M_r for HGJB and PJB with the ambient
328 temperature ($\Lambda = 5$, $\phi_a = 0.9$), together with the evolution of
329 the minimum value of $M_{r,min}$ for $\phi_a = 1$ 29
330 A.13 Void fraction as a function of temperature in the limit case
331 where all the water content condenses ($\phi_a = 1$) 30

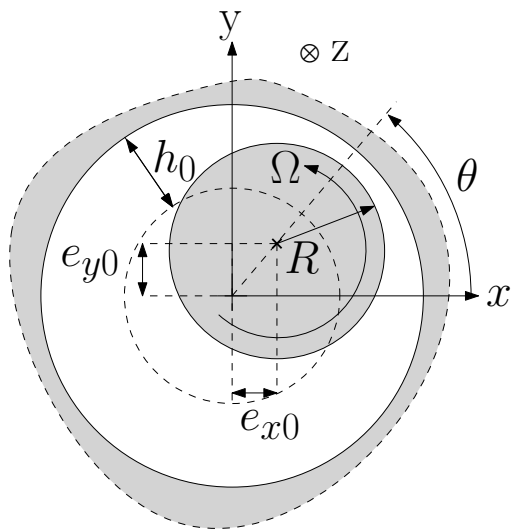


Figure A.1: Nomenclature of a journal bearing

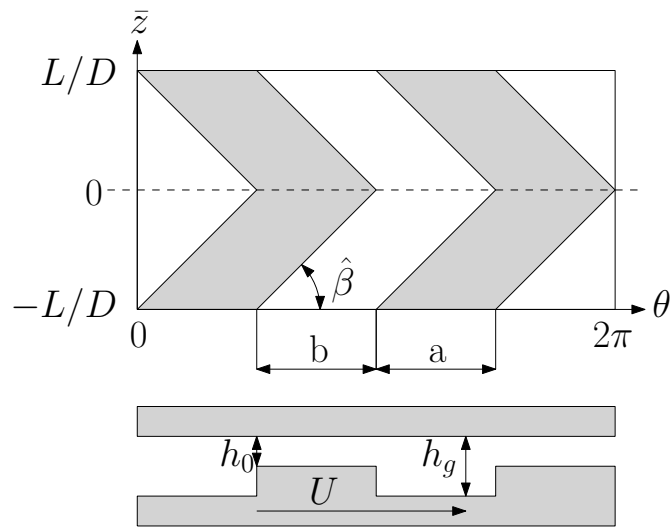


Figure A.2: Geometry and nomenclature of a HGJB

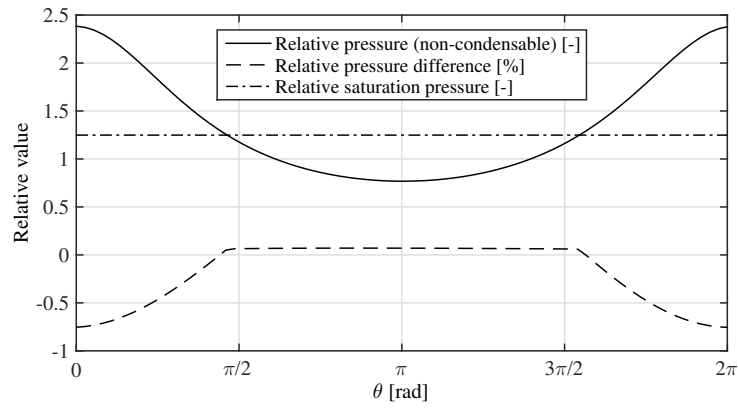


Figure A.3: Relative pressure and deviation along the circumference of a PJB at $\bar{z} = 0$, $\epsilon_x = 0.5$, $\phi_a = 0.8$ and $\Lambda = 30$)

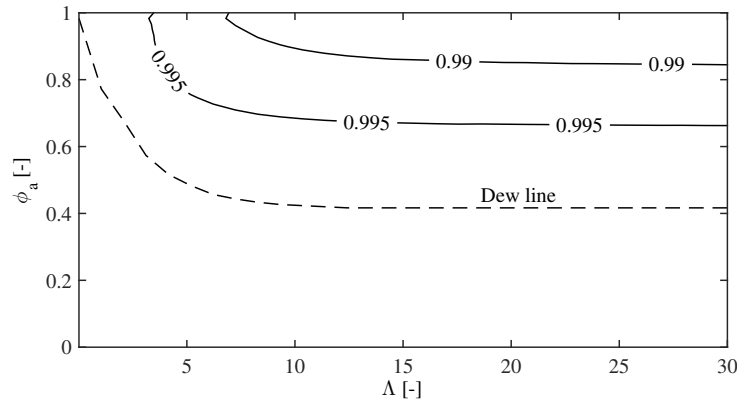


Figure A.4: Isolines of W_r for PJB at $\epsilon_x = 0.5$ ($T_a = 308$ K)

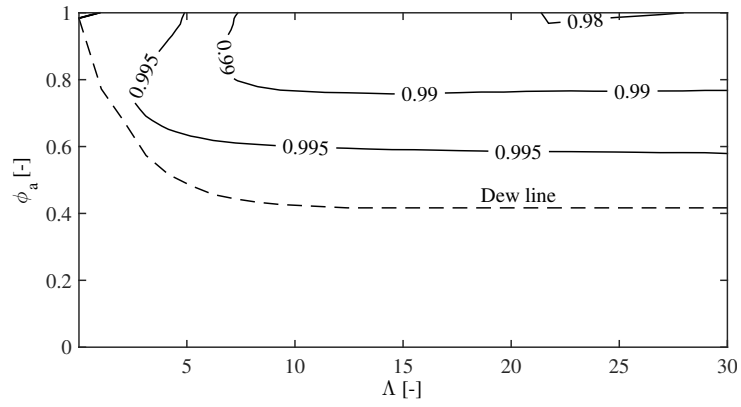


Figure A.5: Isolines of M_r for PJB at $\epsilon_x = 0.5$ ($T_a = 308$ K)

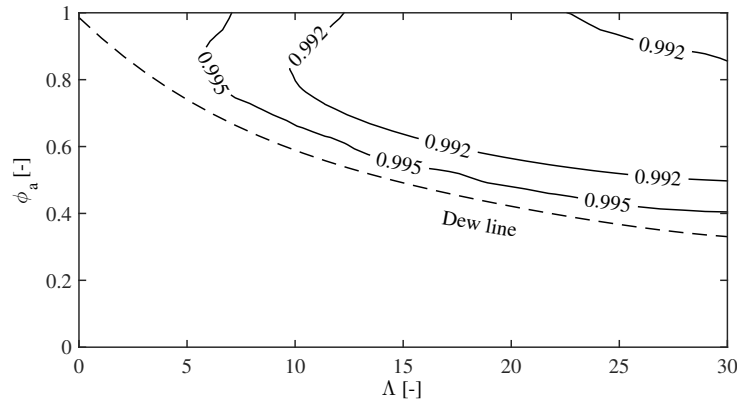


Figure A.6: Isolines of W_r for HGJB at $\epsilon_x = 0.05$ ($T_a = 308$ K)

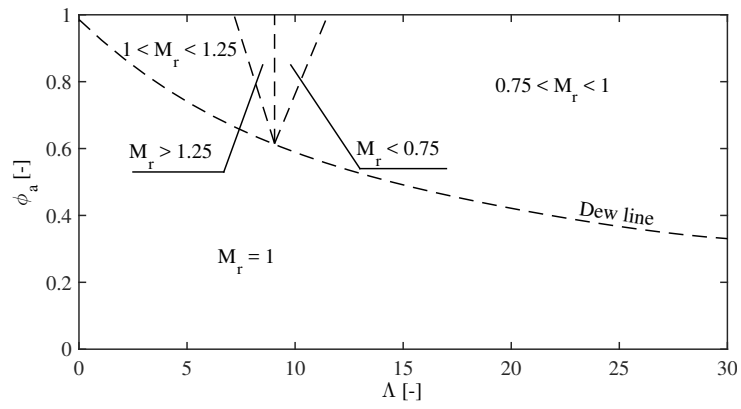


Figure A.7: Isolines of M_r for HGJB at $\epsilon_x = 0.05$ ($T_a = 308$ K)

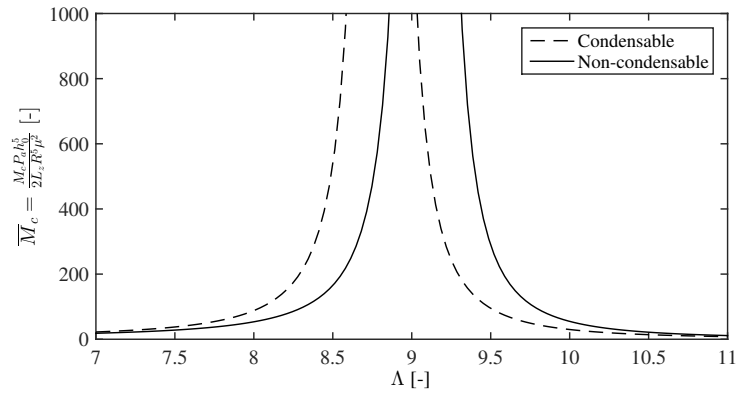


Figure A.8: Critical mass for HGJB at $\epsilon_x = 0.05$ ($T_a = 308$ K, $\phi_a = 1$) as a function of Λ with and without vapor condensation

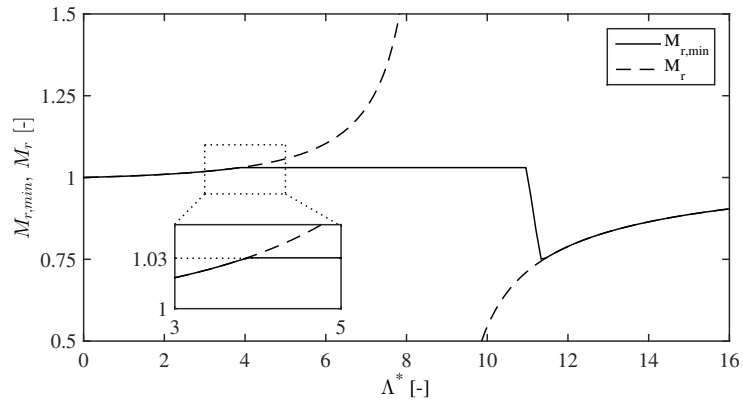


Figure A.9: M_r and $M_{r,min}$ for HGJB at $\epsilon_x = 0.05$ ($T_a = 308$ K, $\phi_a = 1$) as a function of Λ

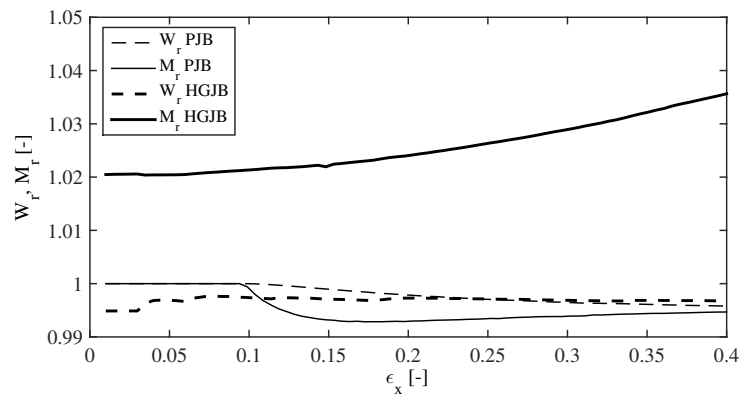


Figure A.10: Evolution of W_r and M_r for HGJB and PJB with the eccentricity ratio ($T_a = 308$ K, $\Lambda=5$, $\phi_a=0.9$)

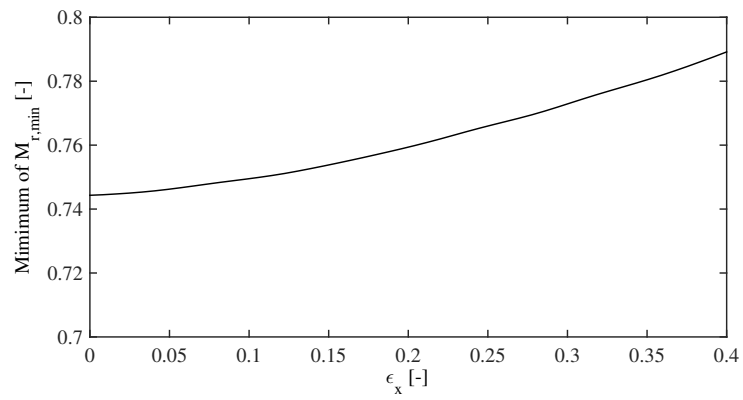


Figure A.11: Evolution of the minimum value of $M_{r,min}$ for $\Lambda^* = 50$ with the eccentricity ratio for HGJB ($T_a = 308$ K, $\phi_a = 1$)

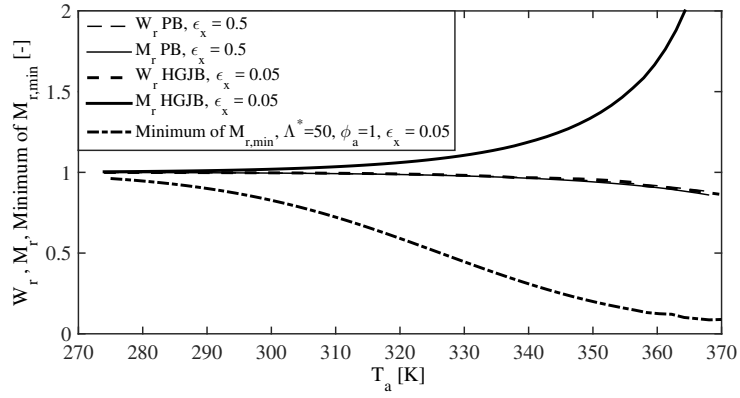


Figure A.12: Evolution of W_r and M_r for HGJB and PJB with the ambient temperature ($\Lambda = 5, \phi_a=0.9$), together with the evolution of the minimum value of $M_{r,\min}$ for $\phi_a=1$

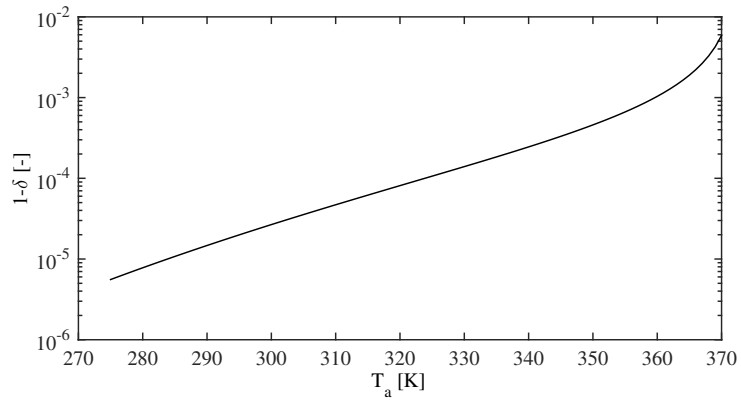


Figure A.13: Void fraction as a function of temperature in the limit case where all the water content condenses ($\phi_a=1$)